analytical chemistry

pubs.acs.org/ac Article

# Dual-Mode SERS and Electrochemical Detection of miRNA Based on Popcorn-like Gold Nanofilms and Toehold-Mediated Strand Displacement Amplification Reaction

Hong Zhou,* Jishou Zhang, Binxiao Li, Jing Liu,* Jing-Juan Xu,* and Hong-Yuan Chen

Cite This: *Anal. Chem.* 2021, 93, 6120–6127 Read Online

ACCESS | Metrics & More | Article Recommendations | Supporting Information

**ABSTRACT:** MicroRNA (miRNA) has emerged as one of the ideal target biomarker analytes for cancer detection because its abnormal expression is closely related to the occurrence of many cancers. In this work, we combined three-dimensional (3D) popcorn-like gold nanofilms as novel surface-enhanced Raman scattering (SERS)-electrochemistry active substrates with toehold-mediated strand displacement reactions (TSDRs) to construct a DNA molecular machine for SERS-electrochemistry dual-mode detection of miRNA. 3D popcorn-like spatial structures generated more active "hot spots" and thus enhanced the sensitivity of SERS and electrochemical signals. Besides, the TSDRs showed high sequence-dependence and high specificity. The addition of target miRNA will trigger the molecular machine to perform two TSDRs in the presence of signal DNA strands modified by R6G (R6G-DNA), thus achieving an enzyme-free amplification detection of miRNA with a low limit of detection of 0.12 fM (for the SERS method) and 2.2 fM (for the electrochemical method). This biosensor can also serve as a universally amplified and sensitive detection platform for monitoring different biomarkers, such as cancer-related DNA, messenger RNA, or miRNA molecules, with high selectivity by changing the corresponding probe sequence.

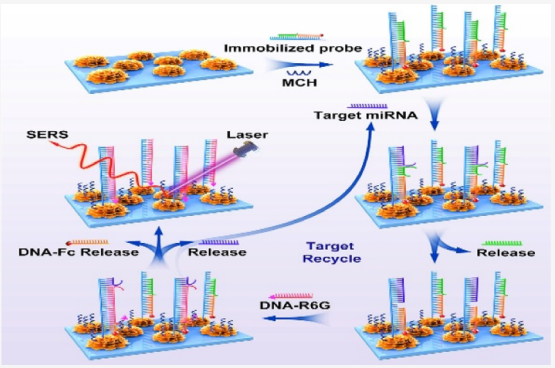




## INTRODUCTION

MicroRNAs (miRNAs) are small RNA molecules widely existing in eukaryotic cells, which regulate the expression of the corresponding miRNA genes. The abnormal expression of miRNA reflects the occurrence and early development of many major diseases, especially cancers. Therefore, as a typical tumor marker, ultrasensitive detection of miRNA is attracting more and more attention and showing increasing importance for the early diagnosis of cancers and the development of targeted anticancer drugs.[1−3] However, due to the small size of miRNA fragments, low expression, and high sequence homology in cells, the ultrasensitive detection of miRNAs faces many challenges using conventional methods,[4] such as microarray analysis techniques,[5] quantitative fluorescence reverse transcription polymerase chain reaction,[6] bioluminescence assays,[7] or northern blotting.[8] In recent years, researchers have introduced signal amplification reactions (such as strand displacement amplification, rolling circle amplification, hybridization chain reaction, etc.) into new technologies (*e.g.*, colorimetric analysis,[9] fluorescence,[10] electrochemiluminescence,[11] chemiluminescence,[12] surface-enhanced Raman,[13] single molecule detection,[14] and electrochemical analysis[15]) and achieved satisfactory ultrasensitive detection of miRNAs.

Among these technologies, electrochemical approaches, benefiting from their advantages of low cost, operation convenience, and relatively high sensitivity, have demonstrated good prospect in the field of miRNA detection.[16] To further improve their performance in sensitivity and stability, many kinds of isothermal amplification technologies and nanomaterials with large surface-to-volume ratios and excellent biocompatibility have been introduced to construct biosensing systems.[17] For example, very recent work by Miao and Tang combined strand displacement amplification technology and dumbbell hybridization chain reaction and presented an electrochemical method for ultrasensitive detection of exosomal miRNA with a detection (LoD) limit as low as the aM level.[18] Using copper- and cobalt-doped $CeO_2$ nanospheres as efficient electrocatalysts, a flexible dual-mode electrochemical biosensor for miRNA was reported which also showed aM level detection level with a wide linear range from 0.1 fM to 10 nM.[19] Besides, noble metal nanoparticles, metal−organic frameworks or doped graphene nanomaterials were widely applied to build ultrasensitive electrochemical bio-

Received: December 14, 2020
Accepted: March 25, 2021
Published: April 6, 2021

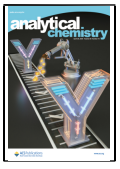




https://doi.org/10.1021/acs.analchem.0c05221
*Anal. Chem.* 2021, 93, 6120–6127

sensors for miRNA.[20−22] SERS technology is used to identify and detect biomolecules using metal nanomaterials and provide nondestructive and sensitive spectral fingerprint information. To date, SERS has also become a promising approach for accurate miRNA detection with high sensitivity and selectivity.[23] These reported methods for miRNA detection mainly used traditional gold flakes as the substrate, which greatly increased costs. Recently, due to the discovery of powerful local electromagnetic field coupling effect between adjacent metal nanostructures, SERS substrates with metal nanostructures have been rapidly developed which generate a strong SERS signal.[24] For example, Cai's group designed a kind of Au octahedral array, which served as a hot spot substrate for let-7a miRNA detection in MCF-7 cell-derived exosomes. Benefiting from the "hot surfaces", the sensitivity was greatly improved to as low as 5.3 aM without using any other signal amplification strategies.[25] To improve the DNA hybridization rate and signal amplification reaction, Ye *et al.* utilized alternating current electrokinetic flow technology for the detection of miRNAs.[26] Their further work also developed ratio-type or dual-signal mode fluorescent-Raman complementary imaging and detection of intracellular miRNA.[27,28] Researchers also found that the morphology of SERS substrates greatly influences the strength of the SERS signal. Therefore, many metals holding unique architectures have been studied for the development of high-performance SERS active substrates for miRNA detection.[29] Among various SERS active structures, three-dimensional (3D) nanostructures (such as star-/flower-like, dendritic morphologies, or sea urchin-like) showed promising performance benefiting from their 3D structures which provide more active "hot spots".[30] For instance, 3D substrates based on sea urchin-like hollow nanostructures have a high surface-to-volume ratio and a rich surface tip. The comparative large active surface area and gap channels could spread the probe molecules into the structure. This greatly improved the efficiency of reactions on the surface.

To further improve the accuracy of detection, SERS often works with other detection techniques to build dual-mode detection techniques. A dual-mode approach shows its great potential application which could provide more convincing information than single signal output approach in the early screening and diagnosis of malignant tumors and other major diseases.[31−34] For example, miRNA, as one of the tumor biomarkers, usually exists in complex biological environments and many very similar gene sequences exist in the same sample. The SERS/electrochemical dual-mode detection method could provide more information from the reactions and thus show more convincing results with greatly reduced false negative/positive detection probability than the single output approach. Besides more accurate results, SERS/electrochemical dual mode detection methods mainly show more flexible detection approaches with two optional support instruments which could cope with different detection conditions as well as flexibly handle different forms (solid or liquid) of samples. However, a SERS/electrochemical dual-mode detection system has been rarely reported.[35] This is mainly because of the high requirement for the design of sensing interface and signal tag which needs to efficiently transmit and respond to the changes of SERS and electrochemical signal from the analyte.

Herein, we constructed electrodeposited popcorn-like Au nanoparticle-FTO glass as a novel SERS substrate for electrochemical sensing interface and combined it with toehold-mediated strand displacement reactions (TSDRs)[36] for the trace detection of miRNA. The proposed strategy has three major advantages. First, the use of 3D nanostructures as substrates enhanced the sensitivity of SERS and electrochemical signals. Second, the highly specific and sequence dependence of the TSDRs results in highly minimized background noise. Third, compared with previous single-signal output sensors, this dual-signal output method provides more accurate quantification detection of the target. The proposed SERS and electrochemical detection method showed excellent performance for the detection of miRNA with a low limit of detection (LoD of 0.12 fM (for the SERS method) and 2.2 fM (for the electrochemical method). Moreover, the utility of this method was further verified by detecting the levels of miRNA in different cancer cells, showing promising application in the field of analysis and detection.

## EXPERIMENTAL SECTION

**Design and Preparation of the FTO-Au NP Chips.** The preparation of the chip is according to the method in our previous work.[37] We first got small pieces of FTO glass (1 cm × 4 cm) by cutting the purchased FTO glass and cleaning by boiling a 2-propanol solution containing 2 M KOH for 20 min. Then, they were washed thoroughly in an ultrasonic bath with ethanol and water and dried at 60 °C. Then, the FTO glass was immersed into 5.0 mL of an electrolyte containing 0.05 M phosphate balanced solution (pH = 2), 0.05 M KCl, and 2.4 mM $HAuCl_4$ solution. Cyclic voltammetry (CV) was constructed with nitrogen gas kept over the electrolyte at 60 °C. The potential was applied from −0.8 to 0.3 V for 50 cycles at 0.05 V/s. Under these conditions, the color of the FTO electrode transformed from colorless into yellow, indicating that Au NPs were deposited on the electrode successfully. Finally, these FTO chips were slightly washed and stored at 4 °C for further experiments.

**Preparation of the Sensors.** 3.0 μM template probes (DNA1 or SH-DNA), 3.2 μM assistant probes (DNA2), and 3.2 μM signal probes (DNA3 or Fc-DNA) were added in Tris−HCl buffer (20 mM, pH 7.4 with 0.1 M NaCl and 25 mM $MgCl_2$). After that, the solution was heated for 10 min at 85 °C, then cooled to 25 °C and kept for 60 min to form duplex probes. 1.0 mM TCEP was added in the above solution and incubated for 1 h to break the disulfide bonds of SH-DNA. Then, 10 μL of the above-formed duplex probes was modified onto the FTO-Au NP chips for 2 h with slight rinsing with phosphate-buffered saline (PBS). After drying with purified nitrogen, the electrodes or FTO-Au NP chips were immersed into 1 mM MCH solution for 2 h, followed by treatment with PBS and nitrogen for use.

**MiRNA Detection with the Recycling Amplification Strategy.** 10 μL of PBS containing different concentrations of miRNA and DNA4 (DNA-R6G, 1.0 μM) was dropped on the substrate (electrodes and FTO-Au NP chips) and incubated for 85 min at room temperature. Then, the electrodes were washed with PBS and transferred to an electrochemical workstation and Raman spectrometer for the following measurements.

**Electrochemical and Raman Spectra Measurements.** Electrochemical impedance spectroscopy (EIS) was conducted on a CHI660B electrochemical workstation (China) in a $K_4Fe(CN)_6/K_3Fe(CN)_6$ (5 mM, 1:1) mixture solution containing 0.1 M KCl. A conventional three-electrode system was used with an Au electrode, a platinum wire, and an Ag/AgCl electrode that served as the working electrode, the


https://doi.org/10.1021/acs.analchem.0c05221
Anal. Chem. 2021, 93, 6120−6127

**Scheme 1. Schematic Illustration of the Proposed Strategy for Enzyme-Free Target Recycling Amplification Detection of miRNA**

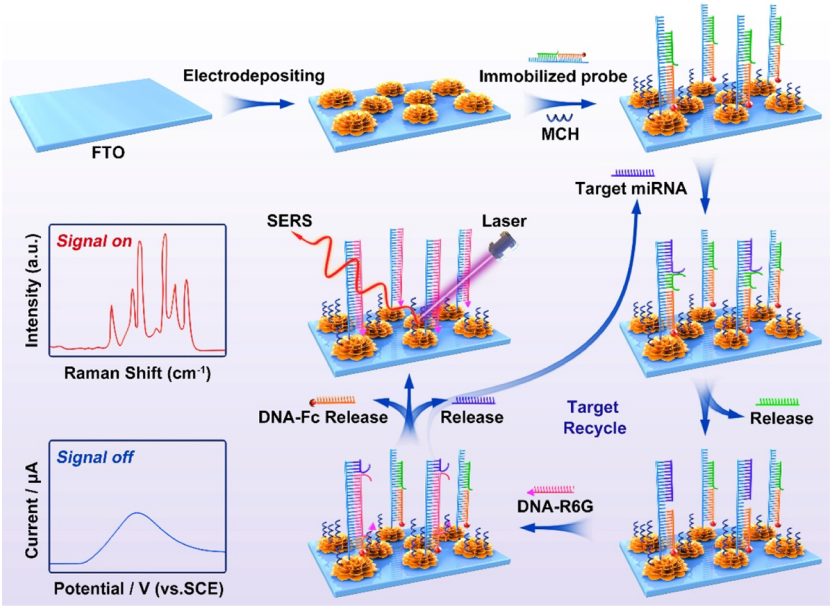


auxiliary electrode, and the reference electrode, respectively. The potential range was 0.1 to 0.6 V under a scan rate of 50 mV $s^{-1}$. Differential pulse voltammetry (DPV) was performed in PBS solution (10 mM, pH 7.4) scanned from 0 to 0.6 V with 50 mV pulse amplitude and 0.2 s pulse period.

After the incubation of the target miRNA and DNA-R6G with FTO-Au NP chips at room temperature and the subsequent air-drying, SERS spectra were measured using a Renishaw inVia Raman spectrometer at 633 nm as the excitation laser. The laser power on the sample was 5 mW, and the accumulation time for every spectrum was 10 s. From different sites, three spectra were collected from every sample and the average represents SERS test results, and the experiments were repeated in triplicate. For SERS mapping, the laser power focused on the target was 10 mW, with 3 s accumulation time and 1 s exposure time. The tip size is 8 $\mu$m and one image contains 200 scanning points. All mapping images use a peak intensity of 1511 $cm^{-1}$ to integrate and the area of the SERS map is 100 $\mu$m × 100 $\mu$m. All SERS mapping images and spectrometer were calibrated with WiRE Raman Software Version 3.4 (Renishaw Ltd.).

## RESULTS AND DISCUSSION

In this study, we used a 3D popcorn-like FTO-Au NP film as the Raman assay substrate. Target miRNA and Rhodamine-6G modified signal strands (R6G-DNA) were employed to initiate two molecular machines constructed by the TSDRs, which were used as platforms for enzyme-free assistant target recycling amplification to achieve highly sensitive SERS detection of miRNA. Scheme 1 shows the principle of this approach. The 3D popcorn-like Au NPs were electrodeposited on FTO glass as Raman-active substrates. Thiolate-modified template probe DNA, electrochemical tag (Fc)-capped signal probe DNA, and the assistant probe DNA strand were mixed and annealed to form double-strand DNA (dsDNA). The formed dsDNA probes were immobilized on a popcorn-like Au NP film *via* Au−S bond with subsequent treatment with MCH solution. DsDNA probes contain two toehold regions in 3′ terminus and the middle of SH-DNA, respectively, providing the opportunity to hybridize with the target miRNA (initiate the first TSDR) and the R6G-DNA strands (initiate the second TSDR), respectively. When target miRNA exists with R6G-DNA in the sensing system, the assistant DNA is displaced because of the hybridization of the miRNA in the first toehold region (the first TSDR). Then, the second toehold region in the middle of SH-DNA is exposed and thus hybridizes with the R6G-DNA. This reaction further displaces the target RNA and Fc-DNA probe (the second TSDR). The released miRNA-21 hybridizes to the first toehold region of SH-DNA again, achieving a target-recycling process which results in a large amount of R6G-DNA binding to the sensor surface and, therefore, a magnified Raman response. Moreover, in the absence of target RNA, the 5′-terminus of thiolate-modified DNA is initially blocked by Fc-DNA and assistant-DNA. This inhibits the generation of TSDRs and then results in a minimal background Raman signal because the R6G-DNA strand will be removed from the surface after washing steps. Therefore, using 3D nanostructures as Raman-active substrates, we realized an amplified Raman signal response for the target analyte and at the same time significantly minimized the background signal in the absence of the target RNA.

**Characterization of the FTO-Au NP Chips.** Figure 1A shows the typical scanning electron microscopy (SEM) image of Au NP films on the FTO glass surface obtained by electrochemical deposition method. We can see that the 3D popcorn-like Au NPs have been successfully electrodeposited on the FTO substrate surface with uniform distribution. The average diameter of the nanoparticles is around 100−400 nm. The inset of its high-magnification SEM image exhibits that these popcorn-like gold nanoparticles were formed *via* the aggregation of tiny nanocrystals. Figure 1B,C shows the SERS bright images and the corresponding SERS intensity mapping (1511 $cm^{-1}$) of the FTO-Au NP substrate (MCH/probe/AuF) in the presence of miRNA and DNA-R6G. As shown in Figure 1B, gold nanoparticles were distributed compactly on the FTO substrate. Additionally, to further evaluate the


https://doi.org/10.1021/acs.analchem.0c05221
Anal. Chem. 2021, 93, 6120−6127

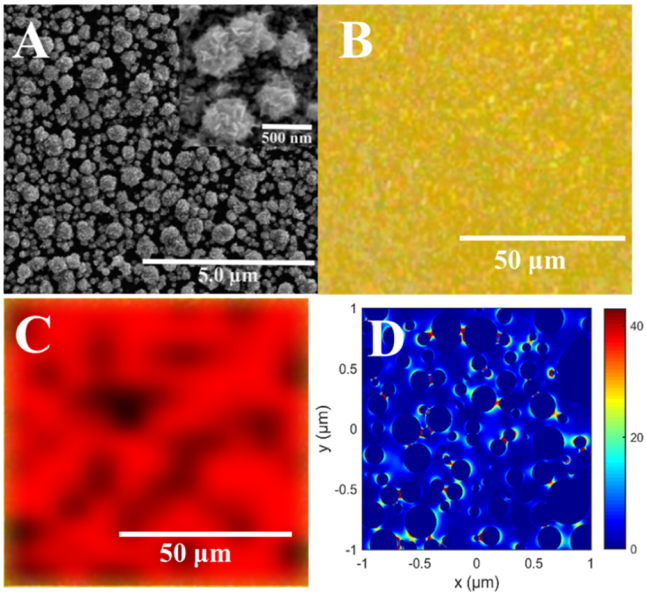


**Figure 1.** (A) SEM and (B) SERS bright images of Au NP films on a FTO glass electrodeposited in $HAuCl_4$ solution (pH 2) containing 0.05 M KCl at 60 °C and with a potential range from −0.8 to 0.3 V for 50 cycles at 50 mV/s by cyclic voltammetry; the inset image of (A) is high-magnification SEM image of Au NPs; (C) SERS intensity mapping (1511 $cm^{-1}$) of the FTO-Au NP substrate (MCH/probe/AuF) in the presence of miRNA (100 nM) and DNA-R6G (1.0 $\mu$M); and (D) electromagnetic field distribution of Au NP films obtained by FDTD simulation at 633 nm.

uniformity of the substrate, SERS mapping images of FTO-Au NP substrate were carried out to evaluate the uniformity across the entire substrate. From Figure 1C, we could see that each pixel represented the Raman intensity of R6G (1511 $cm^{-1}$) at the spatial position on the substrates and the SERS-active sites demonstrated a relatively consistent Raman intensity. Additionally, electric field distributions on the FTO-Au NP substrate are simulated and compared by finite-difference time-domain (FDTD) at 633 nm. As shown in Figure 1D, the local electromagnetic field showed a great enhancement benefit from the hot spot effect near/within the nanogaps on the FTO-Au NP substrate. The results are consistent with the data from SERS intensity mapping (1511 $cm^{-1}$) spectroscopy experiment in Figure 1C. Furthermore, the popcorn-like structures of Au NPs indicated a high surface area to volume ratios which is extremely useful for the construction of biosensors based on enzymes, proteins, or other biological molecules, providing an improved detection sensitivity compared to traditional Au slices.

**Electrochemical Characterization of FTO-Au NP Sensors.** We first used CV and EIS to characterize each step of the fabrication of the FTO-Au NPs. From Figure S1A, we can see a couple of reversible redox peaks from $[Fe(CN)_6]^{3-/4-}$ (curve a) due to the strong electron transfer ability of $[Fe(CN)_6]^{3-/4-}$ to bare FTO-Au NP films (AuF). After the modification of Fc-DNA probes on the Au NP films surface, due to the negatively charged phosphate backbones of the Fc-DNA probe, the electron transfer ability of $[Fe(CN)_6]^{3-/4-}$ was obviously inhibited, exhibiting a decreased redox current and an increased tendency in peak separation (curve b). After further modification of MCH molecules, more significant inhibited current was obtained (curve c). Similar results were obtained with EIS (Figure S1 B). This experimental result reveals the successful fabrication of FTO-Au NP sensors.

**Feasibility of This Strategy.** Strand recycling displacement reactions for amplified detection of miRNA were further tested with DPV and Raman spectroscopy. Figure 2A shows that without DNA-R6G strands and the target miRNA, a significant peak current is obtained on the MCH/probe/AuF sensor in the presence of Fc-DNA. Similarly, the incubation of the sensor with DNA-R6G (MCH/probe/AuF/DNA-R6G) or the target miRNA (MCH/probe/AuF/miRNA) could also obtain a significant peak current because of the inhibition of the strand displacement reactions attachment of the DNA-R6G strands (MCH/probe/AuF/DNA-R6G) without the target miRNA or DNA-R6G strands (MCH/probe/AuF/miRNA).- When both the DNA-R6G strands and target miRNA (MCH/probe/AuF/miRNA/DNA-R6G) are incubated with the sensor, a weak peak current is obtained because of the attachment of DNA-R6G strands on the surface after target-recycling amplification reactions. DNA-R6G displaced the signal probes Fc-DNA and weakened the signal intensity.

Meanwhile, we obtained opposite signal intensity results with Raman spectroscopy. From Figure 2B, almost no SERS signal is observed on the MCH/probe/AuF sensor in the

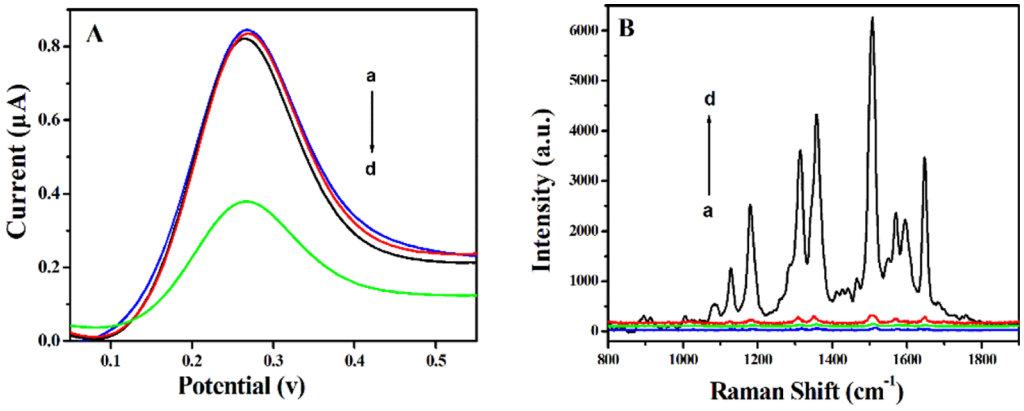


**Figure 2.** (A) DPVs and (B) SERS spectra of (a) MCH/probe/AuF; (b) MCH/probe/AuF/DNA-R6G; (c) MCH/probe/AuF/miRNA; and (d) MCH/probe/AuF/miRNA/DNA-R6G; DPVs obtained in 10 mM PBS (pH 7.4), the pulse amplitude: 50 mV, pulse period: 0.2 s, and scan rate: 100 mV/s; SERS spectra obtained from the feasibility experiment with miRNA-21 (50.0 pM) and DNA-R6G strands (1.0 $\mu$M), excitation: 633 nm, laser power: 5 mW, and acquisition time: 10 s.


https://doi.org/10.1021/acs.analchem.0c05221
Anal. Chem. 2021, 93, 6120−6127

absence of DNA-R6G strands (MCH/probe/AuF/miRNA) and target miRNA (MCH/probe/AuF/DNA-R6G), which further proved that DNA-R6G strands as SERS signal markers cannot attach to SH-DNA without the target miRNA and will be removed away efficiently during washing steps. However, a significant SERS signal is obtained when both the DNA-R6G strands and target miRNA (MCH/probe/AuF/miRNA/DNA-R6G) are incubated with the sensor. The above results clearly illuminate a great potential of this method for sensitive miRNA detection.

To further evaluate the feasibility of the biosensor, we employed native polyacrylamide gel electrophoresis (PAGE) to verify the TSDRs. As shown in Figure 3, lanes 2, 3, and 4

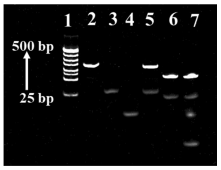


**Figure 3.** PAGE characterization of the TSDR process. Lanes 1−7: marker, probes (DNA1 + DNA2 + DNA3), DNA4, miRNA-21, probe + DNA4, probe + miRNA-21, and probe + DNA4+ miRNA-21. The volume of all samples was 5.0 $\mu$L, and the concentration of DNA was 1.0 $\mu$M.

showed the results from the probes, DNA4, and miR-21, respectively. The lanes 5, 6, and 7 stand for probe + DNA4, probe + miRNA-21, and probe + DNA4+ miRNA-21, respectively. In the mixture of the probe and DNA4, there are only two bands corresponding to probe (lane 2) and DNA4 (lane 3) in lane 5, and no new bright bands appear. This proved that the reaction between the probes and DNA4 will not occur without the target miRNA. However, lane 6 showed two new bands, demonstrating that the target miRNA-21 can hybridize with the probes and release the strand DNA2. Using the mixture of probe, DNA4, and miRNA-21, the TSDR is triggered, DNA2 (the second band in lane 7) is displaced from the probe because of the hybridization of the miRNA, and then DNA1 hybridizes with DNA4 to form a dsDNA product (the first band in lane 7) and further displaces the target miRNA (the third band in lane 7) as well as DNA3 in the probe (the fourth band in lane 7). These results verify the feasibility of these TSDRs.

**Optimization of Detection Conditions.** To achieve the first-rank experimental performance for miRNA detection, the best reaction conditions were explored including the probe DNA concentration and the incubation time. Figure S2 shows the exploration results of the concentration of Fc-DNA and the incubation time of Raman detection in the presence of DNA-R6G strands (1 $\mu$M) and miRNA (50 pM). From Figure S2A, we could find that the current intensity gradually increased with the increase in Fc-DNA concentration. This is due to the fact that more amount of immobilized Fc-DNA results in more electron transfer on the sensor surface, facilitating the increase in current intensity. However, beyond 0.8 $\mu$M, the current intensity tended to be stable. Thus, 0.8 $\mu$M Fc-DNA probes was chosen for the subsequent experiments. Moreover, the incubation time was further examined, which could affect the Raman intensity *via* the reaction efficiency. Figure S2B shows the relationship between the incubation time and Raman signal. We can see the Raman signal had a gradually rising tendency with the increase in time and reached a plateau at 80 min. Thus, 80 min was chosen as the optimal incubation time.

**Reproducibility of the FTO-Au NP Substrate.** To investigate the reproducibility of the FTO-Au N substrate, Raman spectra on different parts of the FTO-Au NP substrate (MCH/probe/AuF) were further tested and compared in the presence of miRNA (0.5 pM) and DNA-R6G (1.0 $\mu$M). As shown in Figure 4A, the hyperspectral SERS intensity distribution map of R6G (1511 $cm^{-1}$) using the FTO-Au NP substrate demonstrates similar spectral features. We randomly recorded Raman spectra of 15 different spots on different parts of the FTO-Au NP substrate. According to Figure 4B, the SERS intensity of these 15 different spots at 1511 $cm^{-1}$ is extremely consistent, with a relative standard deviation of 3.6%. These results indicate that the signal measurements of the fabricated FTO-Au NP substrate showed good reproducibility and thus provide an excellent platform for recycling amplified detection of miRNA.

**Raman Detection of miRNA-21.** We subsequently detected miRNA-21 as a target *via* this method to evaluate its sensitivity. Figure 5A shows the Raman signal 3D curves which show the relationship between the Raman intensity and the concentration of the target miRNA from 0 to 1000 fM. As shown in Figure 5C, a gradual increase in the Raman signal intensity of the peak at 1511 $cm^{-1}$ is observed as the concentrations of the target miRNA ranged from 0.5 fM to 0.5 pM. This increasing trend can also be directly identified in the

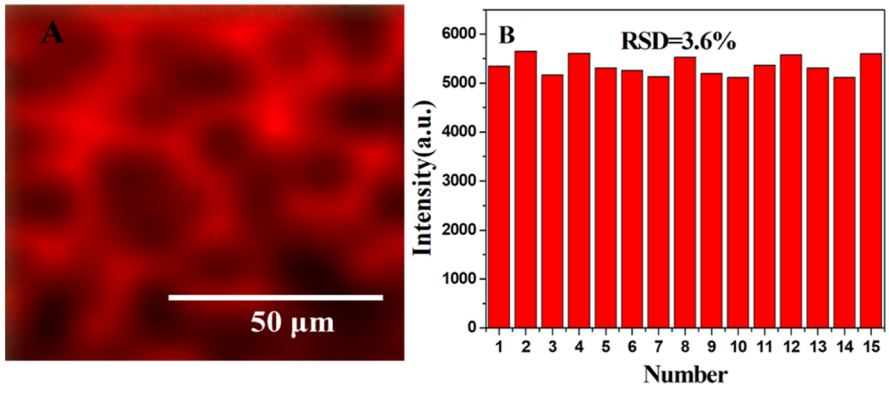


**Figure 4.** (A) SERS intensity mapping (1511 $cm^{-1}$) and (B) histograms illustrating the SERS reproducibility with 15 parts of the FTO-Au NP substrate (MCH/probe/AuF) in the presence of miRNA (0.5 pM) and DNA-R6G (1.0 $\mu$M).


https://doi.org/10.1021/acs.analchem.0c05221
*Anal. Chem.* 2021, 93, 6120−6127

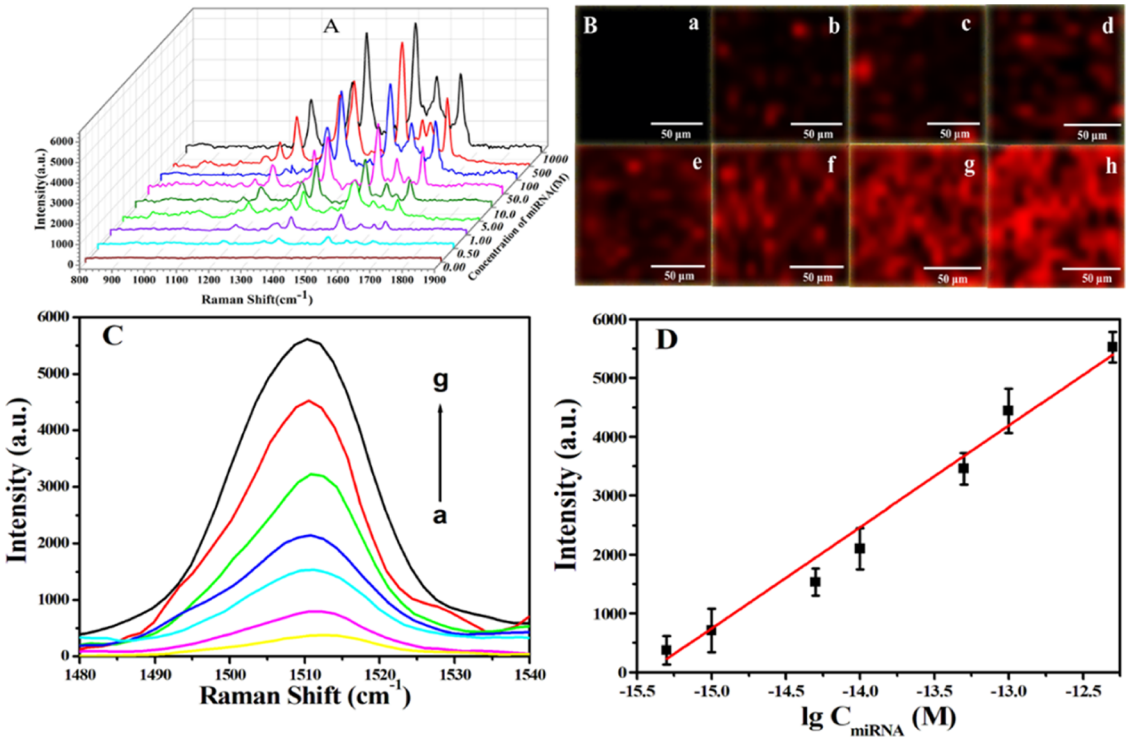


**Figure 5.** (A) SERS spectra variance of Raman intensity with different concentrations of the target miRNA; (B) SERS mapping images with each miRNA concentration (a) 0 (b) 0.5 fM, (c) 1.0 fM, (d) 5.0 fM, (e) 10 fM, (f) 50 fM, (g) 0.1 pM, and (h) 0.5 pM; (C) Raman spectra showing peaks at 1511 cm$^{-1}$ with different concentrations of the target miRNA (a) 0.5 fM, (b) 1.0 fM, (c) 5.0 fM, (d) 10 fM, (e) 50 fM, (f) 0.1 pM, and (g) 0.5 pM; and (D) corresponding linear fitting curve of peak intensity changes for (C). Error bars showed the standard deviation of three experiments.

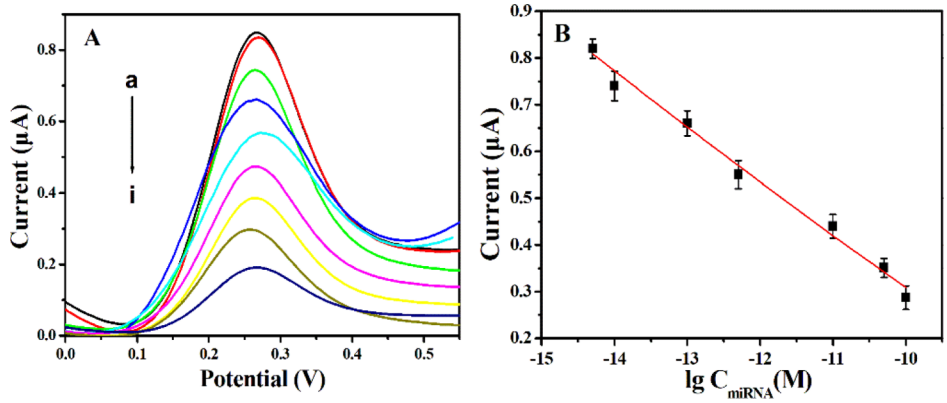


**Figure 6.** (A) Typical DPV responses of the sensors to different concentrations of the target miRNA range from (a−i) (0, 5.0 fM, 10 fM, 0.1 pM, 0.5 pM, 10 pM, 50 pM, 1.0 nM, and 0.5 nM) and (B) corresponding calibration plot for the DPV peak current. Error bars, SD, $n$ = 3.

SERS mapping images (at 1511 cm$^{-1}$) in Figure 5B. Furthermore, a standard curve between the SERS peak at 1511 cm$^{-1}$ and the concentration of the target miRNA, which is corresponding to Figure 5C, exhibited a good correlation coefficient (Figure 5D, $R^2$ = 0.991). The correlation equation was $I$ (a.u) = 1770.18391 log $C$ + 27,169.5537 ($I$ is the Raman peak intensity at 1511 cm$^{-1}$ and $C$ is the concentration of the target miRNA). The detection limit was estimated to be 0.12 fM (S/N = 3). This result indicated the SERS biosensing platform exhibits good performance compared with other methods of miRNA detection (Table S1).

**Electrochemical Detection of miRNA-21.** Finally, the proposed strategy to monitor miRNA with Raman spectroscopy was studied compared to the electrochemical method. Figure 6A shows the current changes of different concentrations of the target miRNA. A greatly weakened current response using a higher concentration of miRNA proved that in the presence of the target miRNA, the Fc-DNA probes were successfully replaced by DNA-R6G strands. Data ranged from 5 fM to 100 pM, showing a good linear relationship between the signal intensity and the logarithm of the target miRNA (Figure 6B). The linear regression equation is $I$ (a.u) = −0.1163 log $C$ − 0.85668 ($I$ is the peak current, $C$ is the concentration of the miRNA-21, and $R^2$ = 0.992). The LoD is estimated to be 2.2 fM (S/N = 3). By comparing the LoD results only, the SERS effect is prominent when using the Raman spectroscopy technique for detection, and the


https://doi.org/10.1021/acs.analchem.0c05221
Anal. Chem. 2021, 93, 6120−6127

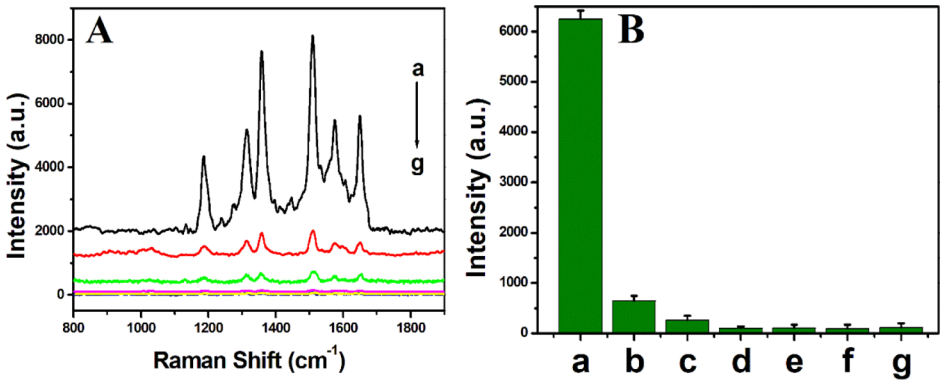


**Figure 7.** Specificity investigation of the proposed method for different miRNA sequences, SERS spectra (A,B) normalized Raman intensity of (a) target miRNA-21 (50.0 pM), (b) single-base mismatch miRNA-21 (5.0 nM), (c) multiple-base mismatches miRNA-21 (5.0 nM), (d) miRNA-210 (5.0 nM), (e) miRNA-155 (5.0 nM), (f) miRNA-126 (5.0 nM), and (g) blank. Error bars, SD, $n$ = 3. Other conditions as in Figure 3.

detection limit was obviously improved compared with the electrochemical method.

**Selectivity and Practical Sample Analysis.** We further confirmed the selectivity of this sensor by employing six miRNA sequences as control (single-base mismatch miRNA-21 and multiple-base mismatches miRNA-21, miRNA-210, miRNA-155, and miRNA-126). As shown in Figure 7, in the presence of the excessive single-base mismatch miRNA-21(5.0 nM), multiple-base mismatches miRNA (5.0 nM), miRNA-210 (5.0 nM), miRNA-155 (5.0 nM), and miRNA-126 (5.0 nM), the Raman signal exhibits negligible change compared with that of the blank sample (the background signal without miRNA-21). In the presence of the target miRNA-21 of much lower concentration (50.0 pM), the SERS intensity is significantly enhanced, which is larger than that of single-base mismatched miRNA (5.0 nM). This clearly demonstrated that the proposed method for miRNA-21 exhibited a good selectivity originating from the highly sequence-dependent property of the strand displacement reactions.

To assess the practical application of this method, two miRNA samples in the lysates from two types of cancer cells, cervical cancer cells (HeLa) and human breast cells (MCF-7), were studied. Figure 8 shows that the lysate from 50 to 500 HeLa cells hardly causes an increase in SERS intensity in comparison to the blank sample without lysate, indicating the low content of miRNA in HeLa cells. However, the lysate from 50 to 500 MCF-7 cells results in a significant increase in SERS intensity, which suggested the high content of miRNA in MCF-7 cells. The above result demonstrates that the content of miRNA in the MCF7 cells is much higher than that in the HeLa cells, and it is well consistent with previous reports.[38−40]

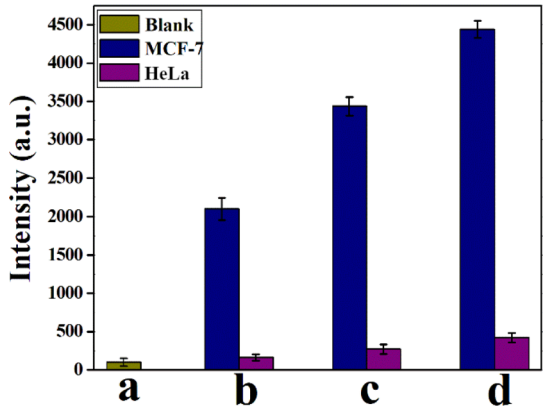


**Figure 8.** Detection of miRNA from two cancer cell lysates: (a) blank solution (in the absence of the target miRNA), (b) MCF7 (50 cells) and HeLa (100 cells), (c) MCF7 (250 cells) and HeLa (250 cells), and (d) MCF7 (500 cells) and HeLa (500 cells).

## CONCLUSIONS

In conclusion, we developed 3D Au-NP films as active SERS-electrochemistry substrates for SERS-electrochemistry dual-mode trace detection of miRNA based on TSDRs. The proposed strategy has three major advantages. First, 3D nanostructure substrates enhanced the sensitivity of SERS and electrochemistry signals. Second, the unique advantages of high sequence dependence of the strand displacement reactions provided highly minimized background noise and an ultrahigh detection limit of 0.12 fM (for the SERS method) and 2.2 fM (for the electrochemical method). Third, compared with previous single-signal output sensors, this dual-signal output method provides more accurate quantification detection of the target. Moreover, the utility of this method was further verified by detecting the levels of miRNA in different cancer cells, showing promising application in the field of analysis and detection.

## ASSOCIATED CONTENT

### Supporting Information

The Supporting Information is available free of charge at https://pubs.acs.org/doi/10.1021/acs.analchem.0c05221.

Reagents and apparatus; details of FDTD simulations; PAGE; cell culture and the process of miRNA extraction; optimization of experimental conditions; and comparison of our strategy with other methods in miRNA detection (PDF)

## AUTHOR INFORMATION

### Corresponding Authors

**Hong Zhou** − *Key Laboratory of Optic-electric Sensing and Analytical Chemistry for Life Science, Ministry of Education, College of Chemistry and Molecular Engineering, Qingdao University of Science and Technology, Qingdao 266042, P. R. China;* orcid.org/0000-0002-9264-7148; Email: zhouhong@qust.edu.cn



https://doi.org/10.1021/acs.analchem.0c05221
*Anal. Chem.* 2021, 93, 6120−6127

**Jing Liu** − *College of Chemical and Biological Engineering, Shandong University of Science and Technology, Qingdao, Shandong 266590, P. R. China*; Email: jliu99@126.com

**Jing-Juan Xu** − *State Key Laboratory of Analytical Chemistry for Life Science, School of Chemistry and Chemical Engineering, Nanjing University, Nanjing 210023, China; College of Chemistry and Molecular Engineering, Zhengzhou University, Zhengzhou 450001, China;* orcid.org/0000-0001-9579-9318; Email: xujj@nju.edu.cn

### Authors

**Jishou Zhang** − *Key Laboratory of Optic-electric Sensing and Analytical Chemistry for Life Science, Ministry of Education, College of Chemistry and Molecular Engineering, Qingdao University of Science and Technology, Qingdao 266042, P. R. China*

**Binxiao Li** − *Department of Chemistry, Shanghai Stomatological Hospital, State Key Laboratory of Molecular Engineering of Polymers and Institute of Biomedical Sciences, Fudan University, Shanghai 200433, P. R. China*

**Hong-Yuan Chen** − *State Key Laboratory of Analytical Chemistry for Life Science, School of Chemistry and Chemical Engineering, Nanjing University, Nanjing 210023, China; College of Chemistry and Molecular Engineering, Zhengzhou University, Zhengzhou 450001, China*

Complete contact information is available at: https://pubs.acs.org/10.1021/acs.analchem.0c05221

### Notes

The authors declare no competing financial interest.

## ■ ACKNOWLEDGMENTS

This work was supported by the National Natural Science Foundation of China (grant no. 21675074) and the Science and Technology Ministry of China (grant no. 2016YFA0201200). This work was also supported by a project funded by the Priority Academic Program Development of Jiangsu Higher Education Institutions.

## ■ REFERENCES

(1) Tricoli, J. V.; Jacobson, J. W. *Cancer Res.* **2007**, *67*, 4553−4555.
(2) Medina, P. P.; Slack, F. J. *Cell Cycle* **2008**, *7*, 2485−2492.
(3) Dong, H.; Lei, J.; Ding, L.; Wen, Y.; Ju, H.; Zhang, X. *Chem. Rev.* **2013**, *113*, 6207−6233.
(4) Ouyang, T.; Liu, Z.; Han, Z.; Ge, Q. *Anal. Chem.* **2019**, *91*, 3179−3186.
(5) Gungormez, C.; Gumushan Aktas, H.; Dilsiz, N.; Borazan, E. *Mol. Biol. Rep.* **2019**, *46*, 4175−4183.
(6) Kloten, V.; Neumann, M. H. D.; Di Pasquale, F.; Sprenger-Haussels, M.; Shaffer, J. M.; Schlumpberger, M.; Herdean, A.; Betsou, F.; Ammerlaan, W.; af Hällström, T.; Serkkola, E.; Forsman, T.; Lianidou, E.; Sjöback, R.; Kubista, M.; Bender, S.; Lampignano, R.; Krahn, T.; Schlange, T.; consortium, C.-I. *Clin. Chem.* **2019**, *65*, 1132−1140.
(7) Cissell, K. A.; Rahimi, Y.; Shrestha, S.; Hunt, E. A.; Deo, S. K. *Anal. Chem.* **2008**, *80*, 2319−2325.
(8) Schwarzkopf, M.; Pierce, N. A. *Nucleic Acids Res.* **2016**, *44*, No. e129.
(9) Zhao, Y.; Gao, X.-Y.; Wang, H.; Wang, J.; Zhou, J.; Zhao, W.; Xu, J.-J.; Chen, H.-Y. *Anal. Chem.* **2019**, *91*, 15988−15992.
(10) Zhang, Y.; Zhang, Y.; Zhang, X.; Li, Y.; He, Y.; Liu, Y.; Ju, H. *Chem. Sci.* **2020**, *11*, 6289−6296.
(11) Zhou, T.; Huang, R.; Huang, M.; Shen, J.; Shan, Y.; Xing, D. *Adv. Sci.* **2020**, *7*, 1903661.
(12) Shen, X.; Xu, W.; Guo, J.; Ouyang, J.; Na, N. *ACS Sens.* **2020**, *5*, 2800−2805.
(13) Liu, C.; Chen, C.; Li, S.; Dong, H.; Dai, W.; Xu, T.; Liu, Y.; Yang, F.; Zhang, X. *Anal. Chem.* **2018**, *90*, 10591−10599.
(14) Li, B.; Liu, Y.; Liu, Y.; Tian, T.; Yang, B.; Huang, X.; Liu, J.; Liu, B. *ACS Nano* **2020**, *14*, 8116−8125.
(15) Li, X.; Li, X.; Li, D.; Zhao, M.; Wu, H.; Shen, B.; Liu, P.; Ding, S. *Biosens. Bioelectron.* **2020**, *168*, 112554.
(16) Liu, L.; Deng, D.; Wu, D.; Hou, W.; Wang, L.; Li, N.; Sun, Z. *Anal. Chim. Acta* **2021**, *1149*, 338199.
(17) Masud, M. K.; Umer, M.; Hossain, M. S. A.; Yamauchi, Y.; Nguyen, N.-T.; Shiddiky, M. J. A. *Trends Biochem. Sci.* **2019**, *44*, 433−452.
(18) Miao, P.; Tang, Y. *Anal. Chem.* **2020**, *92*, 12026−12032.
(19) Xue, S.; Li, Q.; Wang, L.; You, W.; Zhang, J.; Che, R. *Anal. Chem.* **2019**, *91*, 2659−2666.
(20) Azzouzi, S.; Fredj, Z.; Turner, A. P. F.; Ali, M. B.; Mak, W. C. *ACS Sens.* **2019**, *4*, 326−334.
(21) Chang, J.; Wang, X.; Wang, J.; Li, H.; Li, F. *Anal. Chem.* **2019**, *91*, 3604−3610.
(22) Wan, Z.; Umer, M.; Lobino, M.; Thiel, D.; Nguyen, N.-T.; Trinchi, A.; Shiddiky, M. J. A.; Gao, Y.; Li, Q. *Carbon* **2020**, *163*, 385−394.
(23) Sun, Y.; Shi, L.; Mi, L.; Guo, R.; Li, T. *J. Mater. Chem. B* **2020**, *8*, 5178−5183.
(24) Li, D.; Xia, L.; Zhou, Q.; Wang, L.; Chen, D.; Gao, X.; Li, Y. *Anal. Chem.* **2020**, *92*, 12769−12773.
(25) Kang, T.; Zhu, J.; Luo, X.; Jia, W.; Wu, P.; Cai, C. *Anal. Chem.* **2021**, *93*, 2519−2526.
(26) Wang, Z.; Ye, S.; Zhang, N.; Liu, X.; Wang, M. *Anal. Chem.* **2019**, *91*, 5043−5050.
(27) Zhang, J.; Zhang, H.; Ye, S.; Wang, X.; Ma, L. *Anal. Chem.* **2021**, *93*, 1466−1471.
(28) Zhang, N.; Ye, S.; Wang, Z.; Li, R.; Wang, M. *ACS Sens.* **2019**, *4*, 924−930.
(29) Luo, W.; Wu, C.; Huang, S.; Luo, X.; Yuan, R.; Yang, X. *Anal. Chem.* **2020**, *92*, 15573−15578.
(30) Ko, H.; Tsukruk, V. V. *Small* **2008**, *4*, 1980−1984.
(31) Sun, C.; Dong, W.; Peng, J.; Wan, X.; Sun, Z.; Li, D.; Wang, S. *Sens. Actuators, B* **2020**, *325*, 128644.
(32) Song, C.; Li, J.; Sun, Y.; Jiang, X.; Zhang, J.; Dong, C.; Wang, L. *Sens. Actuators, B* **2020**, *310*, 127849.
(33) Zhang, J.; Ma, X.; Wang, Z. *Anal. Chem.* **2019**, *91*, 6600−6607.
(34) Wen, S.; Su, Y.; Dai, C.; Jia, J.; Fan, G.-C.; Jiang, L.-P.; Song, R.-B.; Zhu, J.-J. *Anal. Chem.* **2019**, *91*, 12298−12306.
(35) Sun, J.; Zhao, Y.; Hou, Y.; Li, H.; Yang, M.; Wang, Y.; Sun, B. *New J. Chem.* **2019**, *43*, 13381−13387.
(36) Li, M.-X.; Xu, C.-H.; Zhang, N.; Qian, G.-S.; Zhao, W.; Xu, J.-J.; Chen, H.-Y. *ACS Nano* **2018**, *12*, 3341−3350.
(37) Zhang, H.; Li, B.; Sun, Z.; Zhou, H.; Zhang, S. *Chem. Sci.* **2017**, *8*, 8025−8029.
(38) Zhang, X.; Yang, Z.; Chang, Y.; Qing, M.; Yuan, R.; Chai, Y. *Anal. Chem.* **2018**, *90*, 9538−9544.
(39) Liu, L.; Lu, H.; Shi, R.; Peng, X.-X.; Xiang, Q.; Wang, B.; Wan, Q.-Q.; Sun, Y.; Yang, F.; Zhang, G.-J. *Anal. Chem.* **2019**, *91*, 13198−13205.
(40) Zhao, J.; Luo, J.; Liu, D.; He, Y.; Li, Q.; Chen, S.; Yuan, R. *Sens. Actuators, B* **2020**, *316*, 128139.